Articles

Crystal Structures of Ligand-Bound Saccharopine Dehydrogenase from *Saccharomyces cerevisiae*[†,‡]

Babak Andi, Hengyu Xu,[§] Paul F. Cook, and Ann H. West*

Department of Chemistry and Biochemistry, University of Oklahoma, 620 Parrington Oval, Norman, Oklahoma 73019

Received July 20, 2007; Revised Manuscript Received August 30, 2007

ABSTRACT: Three structures of saccharopine dehydrogenase (L-lysine-forming) (SDH) have been determined in the presence of sulfate, adenosine monophosphate (AMP), and oxalylglycine (OxGly). In the sulfate-bound structure, a sulfate ion binds in a cleft between the two domains of SDH, occupies one of the substrate carboxylate binding sites, and results in partial closure of the active site of the enzyme due to a domain rotation of almost 12° in comparison to the apoenzyme structure. In the second structure, AMP binds to the active site in an area where the NAD^+ cofactor is expected to bind. All of the AMP moieties (adenine ring, ribose, and phosphate) interact with specific residues of the enzyme. In the OxGly-bound structure, carboxylates of OxGly interact with arginine residues representative of the manner in which substrate (α-ketoglutarate and saccharopine) may bind. The α-keto group of OxGly interacts with Lys77 and His96, which are candidates for acid−base catalysis. Analysis of ligand−enzyme interactions, comparative structural analysis, corroboration with kinetic data, and discussion of a ternary complex model are presented in this study.

Saccharopine dehydrogenase (SDH)[1] [N^6-(glutaryl-2)-L-lysine:nicotinamide adenine dinucleotide (NAD^+) oxidoreductase (L-lysine-forming) (EC 1.5.1.7)] is the last enzyme in the α-aminoadipate pathway for L-lysine biosynthesis in the nonpathogenic yeast *Saccharomyces cerevisiae*, some human pathogenic fungi such as *Candida albicans*, *Cryptococcus neoformans*, and *Aspergillus fumigatus*, and plant pathogens such as *Magnaporthe grisea* (1−3). Immunocompromised patients (transplant, cancer, and AIDS patients) are the primary target for these opportunistic pathogenic fungi. In addition, *M. grisea* is one of the most destructive pathogens in crop plants (rice blast) (*4*). Since the α-aminoadipate pathway is unique to fungal organisms, the enzymes in this pathway represent potential targets for the design of new antimycotic agents (*5*).

Saccharopine dehydrogenase catalyzes the reversible oxidative deamination of saccharopine to produce α-ketoglutarate (α-Kg) and lysine using NAD^+ as the oxidant. On the basis of detailed kinetic studies of SDH, an ordered sequential kinetic mechanism was proposed (*6*) with NAD^+ as the first substrate to bind to form an E·NAD^+ binary complex in the physiologic reaction direction. Upon binding of saccharopine to the binary complex, the reaction proceeds through a series of intermediates to give products. In the reverse reaction direction, NADH adds to the enzyme first, followed by random addition of α-Kg and lysine. Detailed inhibition studies suggest that oxaloacetate, glutarate, and lysine can bind to the free enzyme form in dead-end fashion (*6*).

A proton shuttle chemical mechanism was proposed for SDH on the basis of the pH dependence of kinetic parameters, dissociation constants for inhibitors, and isotope effects (*7*). These studies suggest that hydride transfer and hydrolysis of the resulting imine contribute to rate limitation. In the proposed chemical mechanism (Scheme 1), a group with a pK_a of 6.2 accepts a proton from the secondary amine of saccharopine as it is oxidized. The resulting imine of saccharopine is then hydrolyzed via a general-base-catalyzed activation of water. The general base in the hydrolysis reaction has a pK_a of about 7.2 and serves to shuttle a proton between itself and the reactant to give lysine and α-ketoglutarate. The side chain amine of the lysine is then

[†] This work was supported by the Grayce B. Kerr Endowment to the University of Oklahoma (to P.F.C.) and by Grant GM 071417 from the National Institutes of Health (to P.F.C. and A.H.W.).

[‡] The atomic coordinates have been deposited in the Protein Data Bank (PDB) with accession codes 2QRJ, 2QRK, and 2QRL for the sulfate-, AMP-, and oxalylglycine-bound SDH structures, respectively.

* To whom correspondence should be addressed. E-mail: awest@ou.edu. Phone: (405) 325-1529. Fax: (405) 325-6111.

[§] Current address: Fred Hutchinson Cancer Research Center, 1100 Fairview Ave. N., Seattle, WA 98109.

[1] Abbreviations: AMP, adenosine monophosphate; 3-APAD$^+$, acetylpyridine adenine dinucleotide; DTT, dithiothreitol; Hepes, *N*-(2-hydroxyethyl)piperazine-*N*′-(2-ethanesulfonic acid); IPTG, isopropyl β-D-1-thiogalactopyranoside; α-Kg, α-ketoglutarate; NAD^+, β-nicotinamide adenine dinucleotide; NADH, β-nicotinamide adenine dinucleotide reduced form; $NADP^+$, β-nicotinamide adenine dinucleotide 2′-phosphate; Ni−NTA, nickel−nitrilotriacetic acid; NMN^+, nicotinamide mononucleotide; OxGly, oxalylglycine; 3-PAAD$^+$, 3-pyridinealdehyde adenine dinucleotide; PEG, polyethylene glycol; PMSF, phenylmethanesulfonyl fluoride; SDH, saccharopine dehydrogenase; SDS−PAGE, sodium dodecyl sulfate−polyacrylamide gel electrophoresis; thio-NAD^+, thionicotinamide adenine dinucleotide.

10.1021/bi701428m CCC: $37.00
Published on Web 10/16/2007

Scheme 1: Proposed Chemical Mechanism for Saccharopine Dehydrogenase[a]

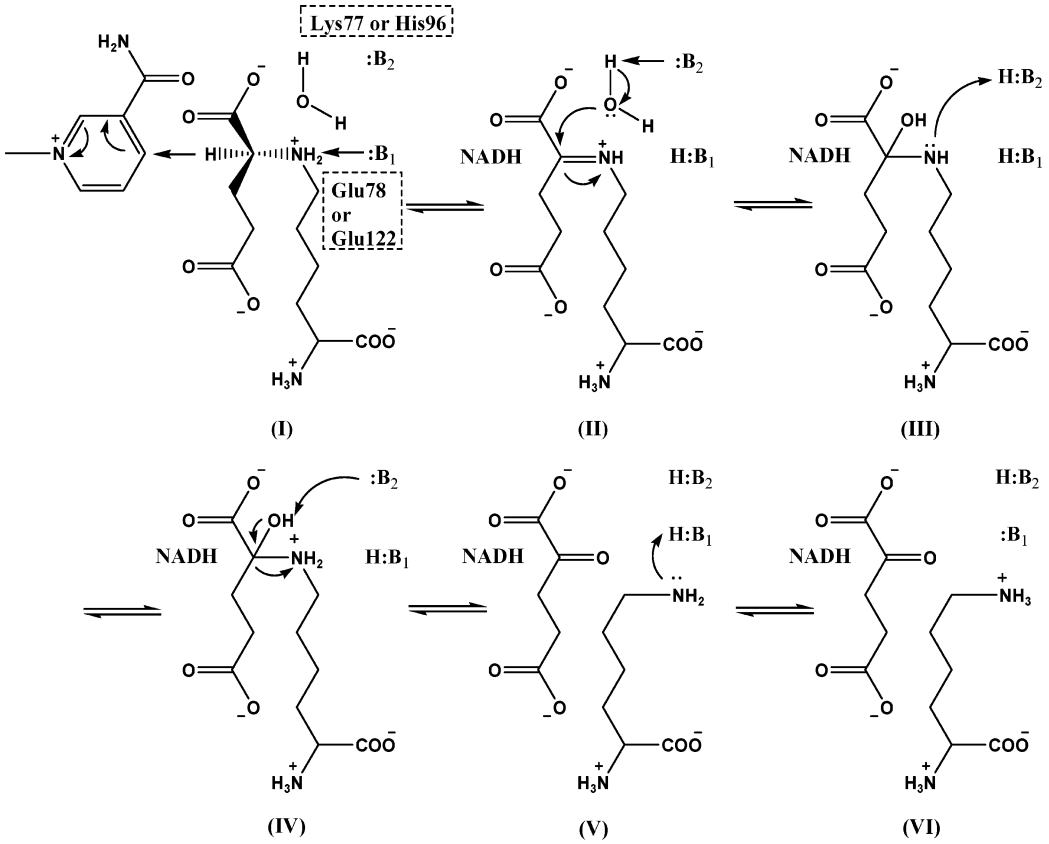

[a] Key: **I**, central complex E·NAD$^+$·saccharopine upon NAD$^+$ and saccharopine binding; **II**, Schiff base intermediate; **III**, carbinolamine intermediate; **IV**, protonated carbinolamine; **V**, generated central complex E·NADH·α-Kg·Lys; **VI**, protonated lysine.

protonated by the acid conjugate of the group with a pK_a of 6.2, and products are released.

A detailed survey of SDH substrate analogues was undertaken to define substrate specificity and to identify the functional groups on all substrates important for binding (*8*). According to this study, a number of NAD$^+$ analogues, including NADP$^+$, 3-acetylpyridine adenine dinucleotide (3-APAD$^+$), 3-pyridinealdehyde adenine dinucleotide (3-PAAD$^+$), and thionicotinamide adenine dinucleotide (thio-NAD$^+$), can serve as substrates. A number of α-keto analogues, including glyoxylate, pyruvate, α-ketobutyrate, α-ketovalerate, α-ketomalonate, and α-ketoadipate, can also serve as substrates for SDH. On the basis of a study of inhibitory analogues (*8*), the majority of the binding energy of the dinucleotide comes from the AMP portion and the α-oxo groups of α-keto acids contribute a factor of 10 to their affinity. Among the inhibitory analogues studied, oxalylglycine showed the highest affinity for SDH with an inhibition constant of 100 μM. Data suggest that the keto acid binding pocket is relatively large and flexible and can accommodate the bulky aromatic ring of a pyridinedicarboxylate. However, a side chain with three carbons (from the α-keto group up to and including the side chain carboxylate) is optimal for binding to the keto acid site. The amino acid binding site is relatively hydrophobic, and the optimal binding length of the hydrophobic portion of the amino acid carbon side chain is three to four carbons (*8*).

The saccharopine dehydrogenase from *S. cerevisiae* consists of 373 amino acids with a calculated molecular weight of 41 464 (Saccharomyces Genome Database (SGD), www.yeastgenome.org). An apparent molecular weight of 39 000 has been reported using gel filtration chromatography, sedimentation equilibrium, and SDS−PAGE, suggesting that SDH from *S. cerevisiae* functions as a monomer (*9*).

The sequence identities between the *S. cerevisiae* SDH and that of pathogenic *C. albicans*, *C. neoformans*, and *A. fumigatus* are 64%, 55%, and 53%, respectively (SGD). Therefore, elucidation of the three-dimensional structure of the *S. cerevisiae* enzyme (in apo and ligand-bound form) is critical for rational design of inhibitors for SDH and the possibility of subsequent antifungal drug therapy for patients infected with pathogenic fungi. Recently, the structure of SDH in the apo form was determined (*10*). The polypeptide chain of saccharopine dehydrogenase from *S. cerevisiae* folds into two similarly sized domains. One of the domains (domain II) is the dinucleotide binding domain known as a Rossmann fold (*11*) that binds NAD$^+$ and NADH. The other domain (domain I) consists of an α/β fold, which is similar to the dinucleotide binding domain in terms of general topology (despite the lack of sequence homology). The active site is located inside a deep cleft at the interface between the two domains (*10*).

In this study, we report ligand-bound (sulfate-, AMP-, and oxalylglycine-bound) crystal structures of saccharopine dehydrogenase from *S. cerevisiae*. A comprehensive analysis with an emphasis on ligand−enzyme interactions, corroboration with previously obtained kinetic data, comparative structural analysis, and a discussion of a semiempirical model of a ternary complex are presented. All three ligand-bound structures presented in this paper are of significant interest

Table 1: Summary of Data Collection Statistics[a]

	sulfate-bound crystal	AMP-bound crystal	OxGly-bound crystal
space group	$C2$ ($\beta = 116.2°$)	$P2_12_12_1$	$P2_12_12_1$
a (Å)	112.63	45.97	64.76
b (Å)	55.21	69.11	74.30
c (Å)	75.04	127.83	74.62
Matthews coeff (Å^3/Da)	2.38	2.31	2.04
solvent content (%)	48.3	46.7	39.7
resolution (Å)	1.60	1.75	1.60
no. of observations	356 114	240 560	295 832
no. of unique reflns	53 059	41 009	46 497
completeness (%)	97.1 (92.9)	97.8 (91.9)	96.5 (87.6)
mean $I/\sigma(I)$	11.3 (3.0)	25.9 (8.8)	15.8 (3.5)
R_{sym}[b] (%)	6.0 (47.7)	3.4 (15.4)	5.6 (35.8)

[a] Values in parentheses correspond to the highest resolution shell. [b] $R_{sym} = \sum(I_j - \bar{I}_j)/\sum(\bar{I}_j)$, where I_j is the intensity measurement for a given reflection and $\bar{I}_j$ is the average intensity for multiple measurements of this reflection.

for rational drug design due to the inhibitory effects of the ligands studied and their similarity to the natural substrates.

MATERIALS AND METHODS

Materials. All chemicals were of the highest grade commercially available. Tris−HCl, Bis-Tris, Hepes, and imidazole were purchased from Research Organics. Ampicillin, isopropyl β-D-1-thiogalactopyranoside (IPTG), $(NH_4)_2SO_4$, KCl, and Coomassie Brilliant Blue G-250 were purchased from Amresco, Gold BioTechnology, EMD, Fisher, and Bio-Rad, respectively. Phenylmethanesulfonyl fluoride (PMSF), chloramphenicol, saccharopine, AMP, and NAD^+ were obtained from Sigma. Sodium acetate was from EM Science. DTT was from Boehringer Mannheim Biochemicals. Oxalylglycine was from Frontier Scientific. PEG 4000 and PEG-MME 2000 were purchased from Fluka and Hampton Research, respectively.

Expression and Purification of the Saccharopine Dehydrogenase. The purification of SDH overexpressed in *Escherichia coli* cells was carried out as reported previously (*6*) with slight modifications. The BL21 (DE3)-RIL *E. coli* cells containing the pSDHHX1 plasmid (a pET-16b derivative) (*6*) with the *LYS1* gene as an insert were grown at 37 °C in 1.5 L of LB medium containing 125 μg/mL ampicillin and 25 μg/mL chloramphenicol. The expression of N-terminal $(His)_{10}$-tagged recombinant SDH was induced by adding 1 mM IPTG at an OD_{600nm} of 0.7−1.0, and incubation was continued for an additional 4.5 h with shaking. The harvested cells were then suspended in 100 mM Tris−HCl, pH 8.0, containing 300 mM KCl and disrupted by sonication using a Misonix model XL2020 sonicator (four alternating 15 s pulse-on and 30 s pulse-off intervals). To prevent proteolysis of SDH, 1 mM PMSF was added to the suspended cells prior to cell lysis. After removal of cell debris by centrifugation at 31000*g* for 10 min, the supernatant was applied to a Ni−NTA column (Qiagen) and eluted using a linear imidazole gradient of 30−300 mM dissolved in the sonication buffer. The purity of the SDH was assessed using SDS−PAGE with the gel stained with Coomassie Brilliant Blue G-250.

Protein Crystallization. The original Crystal Screen kit and Crystal Screen 2 kit from Hampton Research were used to identify initial crystallization conditions using the hanging-drop vapor diffusion method (*13*). Additional homemade screening kits including polyethylene glycols (PEGs) of various molecular weights vs pH and salt additives were also used to explore a range of precipitants and buffer pH. Crystallization trials were performed by mixing 2 μL of the enzyme solution (6−9 mg/mL in 100 mM Tris−HCl, pH 7.0) with the same amount of reservoir (precipitant) solution equilibrated over 0.5 mL of reservoir solution at 4 and 25 °C using 24-well VDX plates (Hampton Research). In addition, purified SDH was shipped to the Hauptman-Woodward Institute (HWI), Buffalo, NY, for screening of their 1536 conditions using the microbatch method under paraffin oil.

Data Collection and Processing. For data collection, crystals were flash-frozen in a stream of nitrogen gas at a temperature of 100 K (Oxford Series 700 cryosystem) in mother liquor containing 15−20% glycerol as a cryoprotectant using MicroMounts from MiTeGen (www.mitegen.com). X-ray diffraction data were collected using Cu Kα radiation ($\lambda = 1.5418$ Å) produced from a Rigaku/MSC RU-H3R rotating anode X-ray generator operated at 50 kV/100 mA and R-Axis IV^{++} image plate detectors. The crystal to

Table 2: Summary of the Refinement Statistics for the SDH Structures

	sulfate-bound structure	AMP-bound structure	OxGly-bound structure
resolution range (Å)	30.0−1.60	30.0−1.75	30.0−1.60
no. of protein atoms	2864	2864	2916
no. of solvent molecules	329 H_2O	358 H_2O	336 H_2O
no. of ligand molecules	3 SO_4^{2-} + 1 Cl^-	1 AMP	1 OxGly
av B factor (all) (Å^2)	28.8	17.0	18.8
av B factor (main) (Å^2)	27.8	16.1	17.9
av B factor (side) (Å^2)	29.8	17.9	19.7
R_{cryst} (R_{free}[a]) (%)	22.1 (25.9)	19.8 (23.3)	20.7 (24.1)
rms deviation			
bond length (Å)	0.016	0.015	0.013
bond angle (deg)	1.47	1.41	1.33
Ramachandran plot (% residues in)			
most favored regions	90.8	90.1	91.2
additional allowed regions	8.9	9.9	8.8
generously allowed regions	0.3	0.0	0.0
disallowed regions	0.0	0.0	0.0

[a] R_{free} was calculated using 5% of the diffraction data.

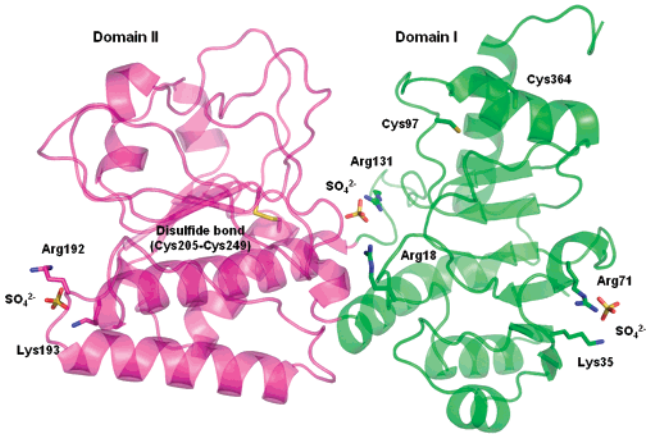

FIGURE 1: Sulfate-bound saccharopine dehydrogenase from *S. cerevisiae*. A ribbon representation of the enzyme monomer shows the positions of bound sulfate molecules. Domain II contains a Rossmann fold (magenta) that binds dinucleotide substrates. The disulfide bond between Cys205 and Cys249 connects the N-terminal end of a helix to a loop that originates from the six-stranded β-sheet core.

detector distance was set at 100 or 120 mm, and data were collected using an oscillation angle of 1°. The exposure time was set to 5 min per image. All data were processed with the d*TREK data processing package (version 9.6D) (*14*).

Molecular Replacement, Model Building, Structure Refinement, and Validation. Structures were solved by molecular replacement using maximum-likelihood techniques (*15*−*17*) as implemented in the program Phaser (version 1.3.1). The candidate model for molecular replacement was the apo-saccharopine dehydrogenase (l-Lys forming) from *S. cerevisiae* (backbone only) (*10*) (PDB code 2Q99). One copy of the candidate model was searched as a single component of the asymmetric unit for the *C*2 and $P2_12_12_1$ space groups. A medium-range resolution dataset of 8.0−3.0 Å was used for both rotation and translation searches.

Automated model building was carried out using ARP/wARP (*18*, *20*) (version 6.1.1) starting from the model obtained from molecular replacement. The initial model was refined by 10 cycles of autobuilding along with five refinement subcycles (total 50 cycles) of REFMAC (*20*) (version 5.2) using the CCP4 program suite (version 6.0.0) (*21*). Manual model building was performed for missing residues using XtalView/Xfit software (version 4.1) (*22*), followed by 10 cycles of maximum-likelihood refinement using REFMAC. The ARP/wARP program was used to add solvent atoms. The quality of the structure factor data and stereochemical properties of the final model were checked using the SFCHECK (*23*) and PROCHECK (*24*) programs implemented in the CCP4 program suite (*21*).

Molecular Graphics. All of the figures in this paper were prepared using PyMOL version 0.99 (*25*).

RESULTS

Expression and Purification of the Saccharopine Dehydrogenase. Expression of SDH in the BL21 (DE3)-RIL *E. coli* cells was very high. The elution profile of the SDH from the Ni−NTA column showed that the enzyme begins to elute at an imidazole concentration of 120 mM, with the highest concentration in fractions eluting at 150 and 180 mM imidazole (data not shown). Eluted SDH fractions estimated

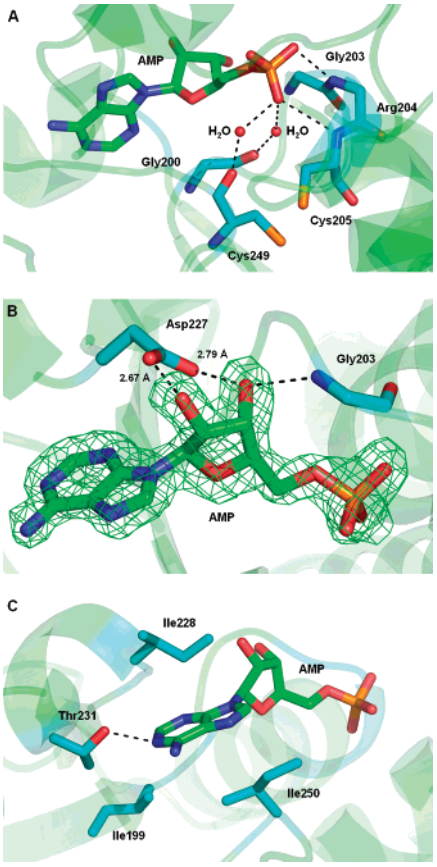

FIGURE 2: Interaction of the AMP molecule with SDH. (A) The phosphate moiety of the AMP interacts solely with the main chain of the enzyme. It interacts directly with N atoms of Arg204 and Cys205 and indirectly through water molecules with O atoms of Gly200 and Cys249. (B) The ribose moiety interacts directly with Asp227 and the main chain N atom of Gly203. The surrounding $F_o - F_c$ electron density for AMP is also shown. (C) Adenine interaction is mainly hydrophobic via Ile199, Ile228, and Ile250. However, Thr231 makes one hydrogen bond to N^1 of adenine.

to be ≥98% pure, on the basis of Coomassie-stained SDS−PAGE gels, were pooled. The amount of purified enzyme obtained typically was 20−27 mg from 1 L of cell culture.

Protein Crystallization. Diffraction-quality single crystals (both in apo and ligand-bound forms) were obtained using homemade screening kits at 4 °C. Apo-SDH crystals usually appeared within 5−7 days with average dimensions of 0.30 × 0.15 × 0.10 mm (rectangular prism). Optimization of the screening solutions resulted in diffraction-quality crystals of apo-SDH in 100 mM Tris (pH 7.0) containing 22% (w/v) PEG 8000 with a final SDH concentration of 3.8 mg/mL in the drop.

A number of $(NH_4)_2SO_4$-containing conditions also gave good-quality crystals for SDH at 4 °C. The highest diffraction-quality crystals grew in 26% (w/v) PEG-MME 2000 in 100 mM Tris, pH 7.0, containing 200 mM $(NH_4)_2SO_4$ (0.29 × 0.35 × 0.05 mm, diamond-like morphology) with a final SDH concentration of 4.5 mg/mL. These crystals were used for data collection and structure determination of the sulfate-bound SDH molecules.

Diffraction-quality AMP-bound crystals were grown using 24% (w/v) PEG-MME 2000 in 100 mM Bis-Tris, pH 6.5, as the precipitant at 4 °C. The final enzyme and AMP concentrations in the crystallization drop were 4.2 mg/mL

and 2.5 mM, respectively. Crystals grew very slowly (40 days) in rod-shaped morphology with a hexagonal cross-section and average dimensions of 0.9 × 0.1 × 0.1 mm.

Oxalylglycine-bound SDH crystals were grown in the presence of 24% (w/v) PEG-MME 2000 in 100 mM Tris, pH 8.0, at 4 °C. The final enzyme and OxGly concentrations in the crystallization drop were 2.4 mg/mL and 10 mM, respectively. The crystallization drop also contained AMP and DTT at final concentrations of 3.0 and 2.5 mM, respectively. The crystals grew as square plates with average dimensions of 0.2 × 0.2 × 0.06 mm.

Data Collection and Processing. Processing of the datasets revealed the space groups to be either $P2_12_12_1$ (for AMP-bound and OxGly-bound) or $C2$ (for sulfate-bound). Molecular replacement using the recently determined apo-SDH structure (*10*) and model refinement were successful in these space groups with the asymmetric unit as a monomer of SDH. A summary of the data collection statistics for all the datasets is shown in Table 1. The space group of the apo-SDH as described by the Berghuis research group is $P2_12_12_1$ with $a = 64.68$ Å, $b = 74.93$ Å, and $c = 74.95$ Å (*10*).

Molecular Replacement, Model Building, Structure Refinement, and Validation. Using the molecular replacement model from Phaser, residues were built using XtalView and ARP/wARP and ligands were added to positions with proper electron density shape and geometry. The first two residues of the protein (Met and Ala) as well as the 21-residue decahistidine tag could not be built due to lack of electron density. The final models were refined using REFMAC. The refinement statistics and features of the final models are summarized in Table 2.

Overall Apo and Ligand-Bound Structures. The overall structure of the apo-SDH enzyme is as described (*10*). It contains two domains of almost the same size. One domain is a Rossmann fold that binds NAD^+/NADH, and the other domain is similar in terms of general topology. Both domains contain a six-stranded parallel β-sheet as a core which is surrounded by α-helices and loops (α/β fold). The two six-stranded β-sheet structures are arranged at almost a 60° angle relative to each other. Cys205 and Cys249 form a disulfide bond in the apo-SDH structure (*10*).

For the sulfate-bound structure, as shown in Figure 1, three sulfate groups bind to one SDH molecule. One sulfate molecule binds to Arg131, which is located in the active site cleft (Arg131 binds to the γ-carboxylate group of oxalylglycine). The other two sulfate molecules bind to arginine and lysine residues in solvent-exposed areas of domains I and II.

For the crystal grown in the presence of 2.5 mM AMP, clear electron density was observed for an AMP molecule in the vicinity of Asp227 (Figure 2B). In addition to the dipole moment of an α-helix perpendicular to the phosphate group, other residues in domain II of the enzyme also play a key role in phosphate binding. As shown in Figure 2A, the phosphate group directly interacts with main chain nitrogen atoms of Arg204 and Cys205. Main chain oxygen atoms of Gly200 and Cys249 are also involved in positioning the phosphate group mediated via two water molecules. Asp227 plays a key role in binding the ribose moiety of the AMP molecule. Both oxygens of the carboxylate of Asp227 are directly involved in hydrogen bonding to the hydroxyl groups of the ribose (Figure 2B). The main chain nitrogen atom of Gly203 also forms a hydrogen bond to the 3′-OH of the ribose moiety of the AMP. The adenine ring is located deep inside a hydrophobic cleft formed by Ile199, Ile228, and Ile250 (Figure 2C). The adenine ring is also held in place by a hydrogen bond between the Thr231 hydroxyl group and the N^1 atom of the adenine ring.

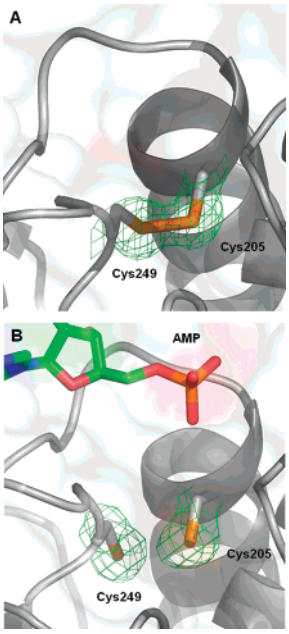

FIGURE 3: View of Cys205 and Cys249, which are involved in disulfide bond formation. (A) Disulfide bond in the sulfate-bound SDH molecule and surrounding $2F_o - F_c$ density. The S−S distance is 2.10 Å. The apo-SDH (*10*) also contained a disulfide bond in a conformation similar to that shown in (A) with a S−S distance of 2.04 Å. (B) Reduced cysteines and their surrounding $2F_o - F_c$ density in the AMP-bound structure.

There is a disulfide bond that forms between Cys205 and Cys249 in SDH. Both apo-SDH and the sulfate-bound SDH structures contain a disulfide bond between these two cysteines (Figure 3A). The S−S distances in the apo and sulfate-bound structures are 2.04 and 2.10 Å, respectively. However, no disulfide bond was observed in the AMP-bound SDH molecule, and the S−S distance is 3.64 Å, which exceeds the van der Waals contact distance of 2.2 Å for two sulfur atoms (Figure 3B).

Figure 4 shows the interaction of oxalylglycine (an α-keto acid inhibitory analogue of α-ketoglutarate) with residues in domain I of the enzyme. Arg18 and Arg131 form ionic bonds with the two carboxylate groups of the OxGly. Lys77 interacts with the α-carboxylate and α-keto groups, while His96 interacts mainly with the α-keto group. The inhibitor also interacts indirectly with Phe135 (main chain) and Ser323 (side chain) through a network of water molecules. The N atom of oxalyglycine has no interaction with any residue on the enzyme. It is predicted that α-ketoglutarate may bind with the same geometry as OxGly to the enzyme active site.

The OxGly-bound crystals were grown in the presence of 3 mM AMP and 2.5 mM DTT. Surprisingly, no AMP molecule was bound to enzyme. Despite using DTT for the crystallization trials, the OxGly-bound structure contained a disulfide bond between Cys205 and Cys249.

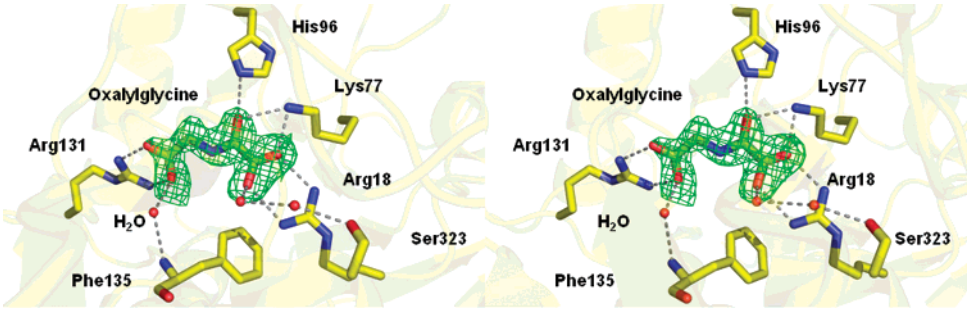

FIGURE 4: Stereoview of the binding of oxalylglycine to the SDH active site. Arg18 and Arg131 are involved in binding the two carboxylate groups of OxGly. Lys77 and His96 interact with the α-keto group, and Lys77 also interacts with α-carboxylate. Phe135 and Ser323 interact indirectly through a water network.

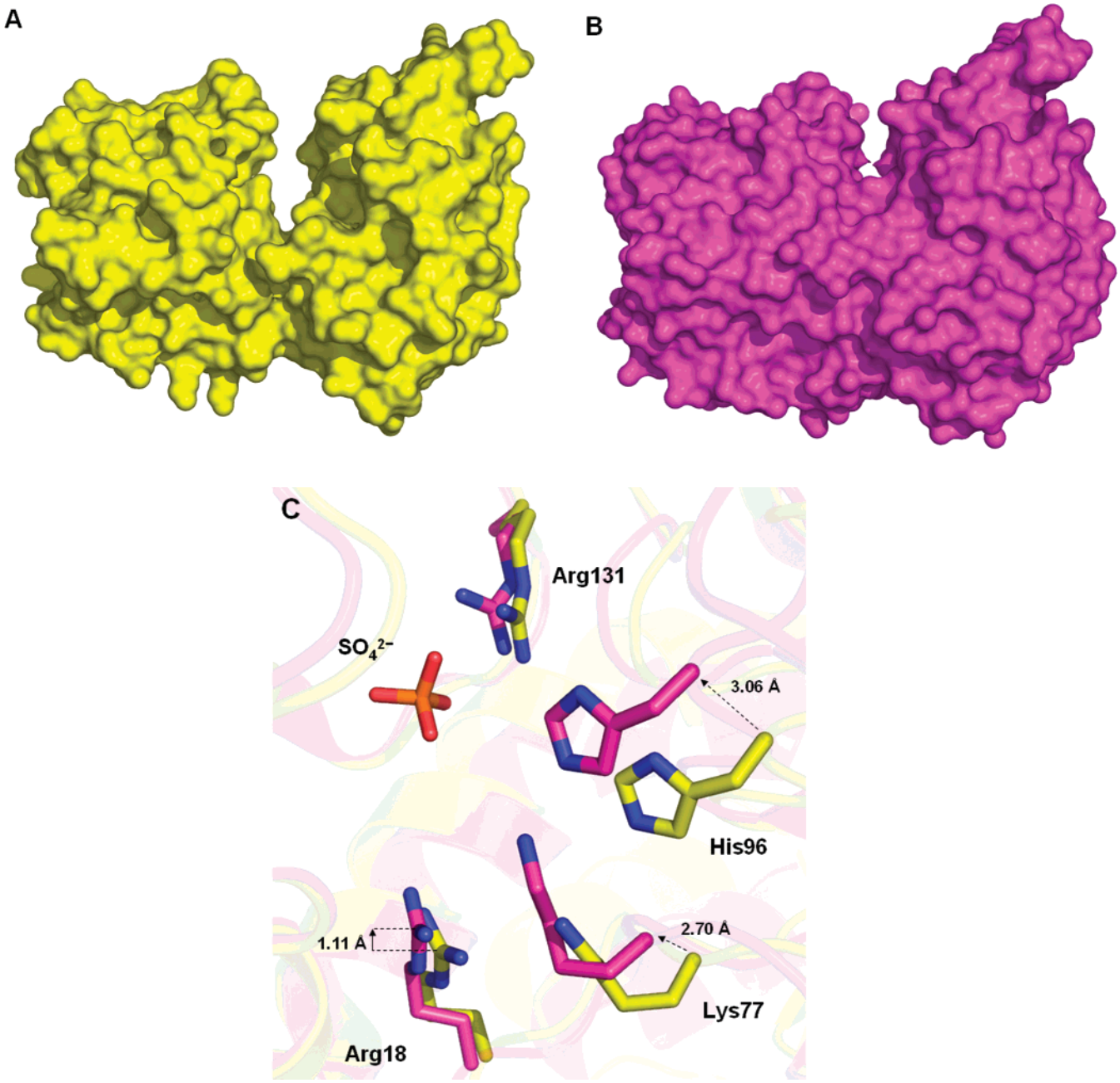

FIGURE 5: Comparative analysis of the apo (yellow) (*10*) and sulfate-bound (magenta) SDH molecules. (A) Surface representation of the apo form of SDH. (B) Binding of a sulfate molecule to Arg131 induces an 11.8° rotation parallel to the plane in one of the domains, leading to 65% closure of the active site. (C) Magnification of the active site area of the superimposed structures of apo (yellow) and sulfate-bound (magenta) SDH shows that conformational changes upon sulfate binding may be triggered by the movement of the Arg18, Lys77, and His96 side chains toward the negatively charged sulfate molecule.

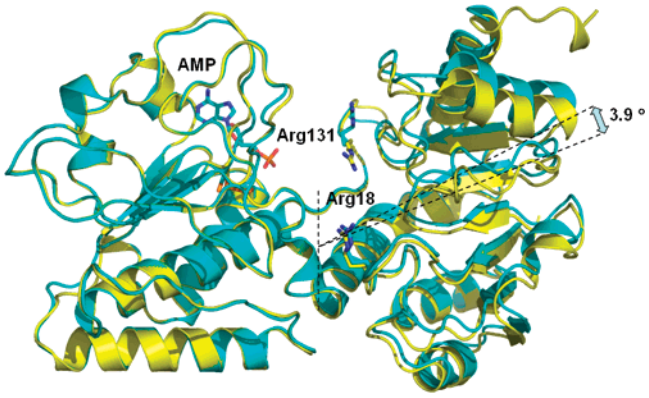

FIGURE 6: Comparative analysis of apo (yellow) (*10*) and AMP-bound (cyan) SDH molecules. A 3.9° rotation of domain I (right) perpendicular to the plane originates from molecular packing in a different unit cell of space group $P2_12_12_1$.

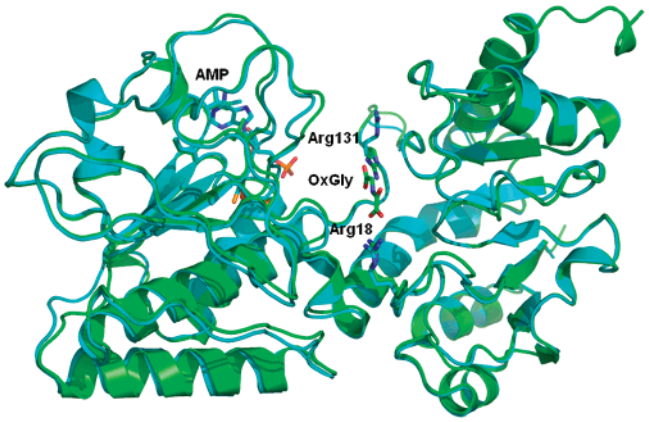

FIGURE 7: Comparative analysis of OxGly-bound (green) and AMP-bound (cyan) SDH molecules. The Rossmann fold (domain II) is specific for binding to dinucleotide substrates, and the other domain (I) is specific for binding to carboxylate-containing substrates or substrate analogues such as α-ketoglutarate, saccharopine, or OxGly.

DISCUSSION

Structural Analysis of the Sulfate-Bound SDH. As shown in Figure 1, sulfate molecules bind to three positions on the SDH enzyme. Binding of sulfate to Arg131 suggests that the sulfate mimics the carboxylate group of the α-keto acid substrate (see the OxGly structure below). Furthermore, binding of sulfate molecules to SDH results in a significant conformational change as shown in Figure 5 and induces the enzyme to crystallize in the *C*2 space group rather than the $P2_12_12_1$ space group (Table 1). According to calculations carried out using the DynDom program for protein domain motion analysis (http://www.sys.uea.ac.uk/dyndom/) (*26*−*28*), there is a rotation of 11.8° between the two domains which leads to 65% active site closure. The hinge residues are predicted to be Ala133-Ala134-Phe135-Gly136 and Leu325-Pro326, with Gly136 and Pro326 being most likely on the basis of superposition of the apo and sulfate-bound structures. Also, both the apo and sulfate-bound structures contain a disulfide bond (Cys205−Cys249) with the same conformational geometry.

The mechanism responsible for active site closure (Figure 5A,B) upon sulfate binding is not known at this time. However, analysis of the structure suggests that electrostatic interactions play a key role. As shown in Figure 5C, the interior surface of the domain that binds sulfate is highly positively charged. Upon binding of a sulfate molecule to Arg131, which functions as an anchor in this interaction, the remaining positively charged residues (Arg18, Lys77, and His96) which are located in a flexible loop area move toward the sulfate molecule (Figure 5C). We suggest that in the case of bound substrates such as saccharopine or substrate analogues such as OxGly, these residues may electrostatically interact with the substrate. The sum of these conformational changes (Figure 5C) results in an 11.8° rotation of the sulfate-bound domain (parallel to the plane) relative to the Rossmann fold, giving rise to 65% active site closure. Although the crystal structure of a ternary complex (SDH·NAD^+· saccharopine) that takes all of the enzyme and substrate conformational changes into account is required to observe the conformational changes relevant to catalysis, the structure of the sulfate complex presented here may provide some preliminary information about the conformational changes relevant to catalysis. This will be discussed further together with the semiempirical model of the ternary complex.

Structural Analysis of the AMP-Bound SDH. The mode of AMP binding to the SDH molecule is consistent with the experimentally determined low K_i value (55 ± 6 μM) (*8*). As shown in Figure 2, eight hydrogen bonds and three hydrophobic residues are involved in AMP binding to SDH. Such a network of hydrogen bonds to the AMP molecule is responsible for the majority of the binding energy of the dinucleotide as previously suggested (*8*). A K_i value of 7.2 ± 0.6 mM is obtained for the NMN^+ molecule (*8*), suggesting that this portion of NAD^+ does not bind with significant affinity to SDH. Despite efforts to cocrystallize SDH in the presence of NMN^+, NAD^+, and NADH, no promising crystals were obtained, likely due to their weak binding or inappropriate crystallization conditions. According to the kinetic data (*8*), the AMP portion of NAD^+ may bind first to the SDH active site. However, it is not clear at this time whether the AMP portion may organize the active site for optimum binding of the NMN^+ portion of the NAD^+ or simply provide the initial interaction.

Hydrogen bonding of the ribose moiety of the AMP molecule to Asp227 contributes to the tight binding and is consistent with the kinetic studies (*8*). It can be concluded from Figure 2B that Asp227 can still form two hydrogen bonds to the ribose moiety of $NADP^+$ with the 2′-phosphate rotated away from the binding site. Structurally, there is no steric hindrance for binding of 2′-phosphate. In agreement, the K_i values for both NAD^+ and $NADP^+$ are about the same (*8*). Asp227, which is involved in hydrogen bonding to the ribose moiety of AMP, is 20 residues C-terminal to the conserved GXXGXXG motif, suggesting that the Rossmann fold of SDH shows the characteristics of a classical NAD-$(P)^+$ binding domain (*29*−*30*).

On the basis of the pH dependence of the K_i for AMP (*8*), two functional groups on the enzyme (one protonated and one unprotonated) are important for AMP binding. According to the crystal structure of the AMP-bound SDH, the unprotonated group is Asp227. The nature of the protonated group is not known, and its identity will require further study.

Apo (*10*) and AMP-bound forms of the enzymes crystallized in the same space group but with different cell dimensions (Table 1). As shown in Figure 6, there are slight

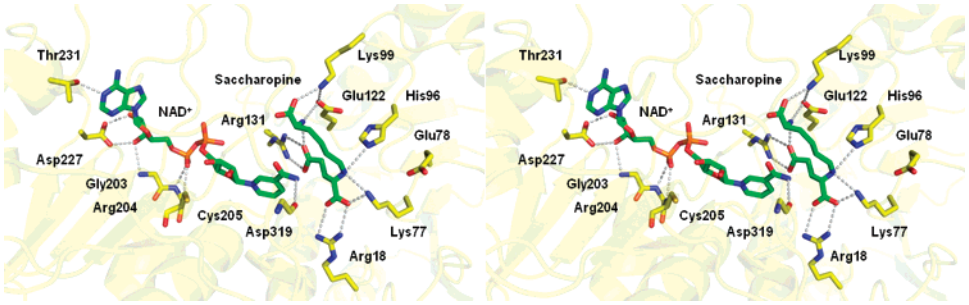

FIGURE 8: Semiempirical model for the SDH·NAD^+·saccharopine ternary complex. All of the interactions between enzyme residues and saccharopine are shown in gray dotted lines (average distance is 2.96 ± 0.18 Å). It is proposed that Glu78 or Glu122 (:B_1 in Scheme 1) and Lys77 or His96 (:B_2 in Scheme 1) are involved in SDH enzymatic catalysis. In the model, saccharopine may form an intramolecular electrostatic bond, which folds the saccharopine onto itself to accommodate the substrate in the highly hydrophilic SDH active site and to minimize the binding energy by intramolecular hydrophobic interaction between the aliphatic segments of lysine and the glutamate moiety of the saccharopine. The nicotinamide ring of NAD^+ presents its *pro-R* face for hydride transfer. The distance between C4 of nicotinamide and C4 of saccharopine is 4.7 Å, suggesting the necessity of a hingelike conformational change for active site closure and catalysis.

conformational differences in both domains. In the AMP-bound structure, there is a 3.9° rotation of domain I (calculated using the DynDom program) which is perpendicular to the plane (Figure 6).

Structural Analysis of the OxGly-Bound SDH. Oxalylglycine is an analogue of α-ketoglutarate that binds to SDH with a K_i of 100 μM (*8*). The crystal structure of the OxGly-bound SDH (Figure 4) shows that the α- and γ-carboxylates of OxGly interact with Arg18 and Arg131, respectively. Although two to six carbons containing substrates can be accommodated, the optimum number of carbon atoms that can be accommodated between Arg18 and Arg131 is five, as predicted by kinetic data (*8*). However, the α-keto group contributes a factor of 10 in binding of α-ketoglutarate or OxGly to the enzyme when compared to the K_i of glutarate (1.0 ± 0.1 mM) (*8*). In the crystal structure, the α-keto group of OxGly accepts hydrogen bonds from Lys77 and His96 with bond lengths of 2.81 and 3.03 Å, respectively (Figure 4). Lys77 and His96 are candidates for the general-base catalyst in the SDH chemical mechanism (*7*).

As shown in the Figure 7, the Rossmann domain is specific for binding to dinucleotide substrates and the other domain is specific for binding to carboxylate-containing substrates and substrate analogues such as α-ketoglutarate, saccharopine, and OxGly. As predicted by kinetic data (*8*), the α-Kg (or OxGly) binding site can easily accommodate the bulky aromatic ring of pyridine-2,4-dicarboxylate (K_i = 1.10 ± 0.01 mM). The side chain of Phe135 may establish hydrophobic interactions with the pyridine ring. However, on the basis of the OxGly binding site as shown in Figure 4, one of the carboxylate groups of pyridine-2,3-dicarboxylate may not be in an optimum position to interact with Arg131 or may sterically clash with the Phe135 side chain, consistent with its higher K_i value (18.3 ± 0.4 mM) relative to that of pyridine-2,4-dicarboxylate. The backbone of Phe135 and side chain hydroxyl of Ser323 also interact indirectly with OxGly through water molecules. The nitrogen atom of OxGly does not make an interaction with any residue on the enzyme and does not contribute to binding. However, the presence of the amide of OxGly limits conformational degrees of freedom for the OxGly molecule, which may explain the better binding of OxGly to SDH than the natural substrate α-ketoglutarate (K_i = 0.6 ± 0.1 mM for the E·NADH·α-Kg complex (*8*)).

Both apo-SDH and OxGly-bound SDH crystallize in the same space group ($P2_12_12_1$) with the same cell dimensions (apo, a = 64.68 Å, b = 74.92 Å, and c = 74.95 Å (*10*); OxGly-bound, a = 64.76 Å, b = 74.30 Å, and c = 74.62 Å). Structural analysis shows that there is no significant domain movement between the two structures (not shown). In the apo-SDH structure (*10*), the OxGly binding pocket is occupied by a network of water molecules connecting Arg18 to Arg131.

Disulfide Bond. Cys205 and Cys249 are located on the surface of the nucleotide binding domain. The structure of the AMP-bound SDH shows that these two cysteines are very close to the phosphate moiety of AMP. On the basis of the crystal structures of the apo-SDH (*10*) and sulfate-bound SDH, Cys205 and Cys249 are involved in disulfide bond formation. The location of Cys205 and Cys249 on the surface of SDH and their juxtaposition presumably make them vulnerable to oxidation during the process of protein purification. It would be expected that, in vivo, disulfide bond formation in SDH would be inhibited due to the highly reducing environment of the cytoplasm. In addition, thioredoxin reductase is a cytoplasmic enzyme that actively prevents the formation of disulfide bonds among cytoplasmic proteins (*31*). Although it is unlikely that the disulfide bond has physiologic importance, this aspect is currently being studied using site-directed mutagenesis.

Semiempirical Model for Substrate Binding and Chemical Mechanism. On the basis of the superposition of the experimentally determined crystal structures of the ligand-bound SDH (AMP- and OxGly-bound), a model of the SDH·NAD^+·saccharopine ternary complex is presented in Figure 8. The model is semiempirical because the lysine moiety of saccharopine and NMN^+ moiety of NAD^+ are modeled. Also, it does not take into account any conformational changes that may arise when both substrates bind to the enzyme (including the closure of the active site) as well as any synergistic interactions. However, the presented model is compatible with the detailed kinetic studies that have been previously carried out for SDH (*6*−*8*). As shown in the model, the carboxylates of the glutamate moiety of the saccharopine make electrostatic and hydrogen-bonding interactions with Arg18 and Arg131. Lys77 and His96 directly interact with the secondary amine of saccharopine. Lys99, Glu122, and the lysine moiety of the saccharopine make a

network of electrostatic and hydrogen bonds. We also propose that there is an intramolecular electrostatic interaction within the saccharopine molecule. The nicotinamide ring of the NAD^+ molecule is in a position to accept a hydride on the *pro-R* face (*8*). In the proposed model, the distance between the C4 of the nicotinamide ring of NAD^+ and the C4 of saccharopine is 4.7 Å, which is longer than the optimum distance of 2.6−3 Å for hydride transfer. Therefore, a hingelike conformational change, as observed in the sulfate-bound structure, may be required to close the active site for catalysis to occur.

A proton shuttle chemical mechanism has previously been proposed for the enzymatic reaction of SDH (*7*). As shown in Scheme 1, in the direction of lysine formation two groups serve as general-base catalysts in the reaction. A general base ($:B_1$) accepts a proton from the secondary amine of saccharopine as it is oxidized and remains protonated until lysine is formed at the completion of the reaction. A second general base ($:B_2$), which shuttles a proton between itself and the reactants, accepts a proton from water as it attacks the Schiff base carbon (**II**) to form the carbinolamine intermediate (**III**). The same residue ($H:B_2$) serves as a general acid and donates a proton to the carbinolamine nitrogen to give protonated carbinolamine (**IV**), and ($:B_2$) then serves as a general base to accept a proton from the carbinolamine hydroxyl to generate α-Kg and lysine (**V**). The ϵ-amine of lysine is then protonated by the group ($H:B_1$) that originally accepted a proton from the secondary amine of saccharopine in the oxidation step (**VI**).

On the basis of the semiempirical model presented in Figure 8, the identity of the group that accepts a proton from the secondary amine of saccharopine ($:B_1$) is either Glu78 or Glu122. The identity of the general-acid−base catalyst ($:B_2$) that catalyzes most of the enzymatic reaction of SDH is either Lys77 or His96. However, the identity of the catalytic groups will have to await further studies.

Elucidation of the crystal structures of the apo (*10*) and ligand-bound forms of saccharopine dehydrogense from *S. cerevisiae* presented in this paper as well as the detailed kinetic studies described (*6*−*8*) is a promising step toward the rational design of antimycotic agents. The final goal is the inhibition of SDH and the lysine biosynthetic pathway in opportunistic pathogenic fungi. Efficient inhibitors can be designed on the basis of the AMP and OxGly binding modes observed in the crystal structures presented here.

ACKNOWLEDGMENT

We are indebted to Dr. Albert M. Berghuis (McGill University, Montreal, Quebec, Canada) for generously providing us with the PDB coordinates for apo-SDH prior to publication and for his insightful discussions on the SDH structure. We are grateful to Bryan Prince for assistance in data collection. We also thank Dr. Daniel M. Copeland and Dr. Xiadong Zhao for their helpful discussions of the crystal structures.

REFERENCES

1. Xu, H., Andi, B., Qian, J., West, A. H., and Cook, P. F. (2006) The α-aminoadipate pathway for lysine biosynthesis in fungi, *Cell Biochem. Biophys. 46*, 43−64.
2. Zabriskie, T. M., and Jackson, M. D. (2000) Lysine biosynthesis and metabolism in fungi, *Nat. Prod. Rep. 17*, 85−97.
3. Garrad, R. C., and Bhattacharjee, J. K. (1992) Lysine biosynthesis in selected pathogenic fungi: Characterization of lysine auxotrophs and the cloned *LYS1* gene of *Candida albicans*, *J. Bacteriol. 174*, 7379−7384.
4. Talbot, N. J. (1995) Having a blast: exploring the pathogenicity of *Magnaporthe grisea*, *Trends Microbiol. 3*, 9−16.
5. Johansson, E., Steffens, J. J., Lindqvist, Y., and Schneider, G. (2000) Crystal structure of saccharopine reductase from *Magnaporthe grisea*, an enzyme of the alpha-aminoadipate pathway of lysine biosynthesis, *Structure 8*, 1037−1047.
6. Xu, H., West, A. H., and Cook, P. F. (2006) Overall kinetic mechanism of saccharopine dehydrogenase from *Saccharomyces cerevisiae*, *Biochemistry 45*, 12156−12166.
7. Xu, H., Alguindigue, S. S., West, A. H., and Cook, P. F. (2007) A proposed proton shuttle mechanism for saccharopine dehydrogenase from *Saccharomyces cerevisiae*, *Biochemistry 46*, 871−882.
8. Xu, H., West, A. H., and Cook, P. F. (2007) Determinants of substrate specificity for saccharopine dehydrogenase from *Saccharomyces cerevisiae*, *Biochemistry 46*, 7625−7636.
9. Ogawa, H., and Fujioka, M. (1978) Purification and characterization of saccharopine dehydrogenase from baker's yeast, *J. Biol. Chem. 253*, 3666−3670.
10. Burk, D. L., Hwang, J., Kwok, E., Marrone, L., Goodfellow, V., Dmitrienko, G. I., and Berghuis, A. M. (2007) Structural studies of the final enzyme in the α-aminoadipate pathway—saccharopine dehydrogenase from *Saccharomyces cerevisiae*, *J. Mol. Biol. 373*; 745−754.
11. Rossmann, M. G., Liljas, A., Branden, C. I., and Banaszak, L. J. (1975) Evolutionary and structural relationship among dehydrogenases, *Enzymes 11*, 51−102.
12. Creighton, T. E. (1989) *Protein structure a practical approach*, pp 157−158, IRL Press, Oxford University Press, Oxford, U.K.
13. McPherson, A. (1999) *Crystallization of biological macromolecules*, pp 159−214, Cold Spring Harbor Laboratory Press, Cold Spring Harbor, NY.
14. Pflugrath, J. W. (1999) The finer things in X-ray diffraction data collection, *Acta Crystallogr. D55*, 1718−1725.
15. Read, R. J. (2001) Pushing the boundaries of molecular replacement with maximum likelihood, *Acta Crystallogr. D57*, 1373−1382.
16. Storoni, L. C., McCoy, A. J., and Read, R. J. (2004) Likelihood-enhanced fast rotation functions, *Acta Crystallogr. D60*, 432−438.
17. McCoy, A. J., Grosse-Kunstleve, R. W., Storoni, L. C., and Read, R. J. (2005) Likelihood-enhanced fast translation functions, *Acta Crystallogr. D61*, 458−464.
18. Lamzin, V. S., and Wilson, K. S. (1993) Automated refinement of protein models, *Acta Crystallogr. D49*, 129−147.
19. Perrakis, A., Morris, R., and Lamzin, V. S. (1999) Automated protein model building combined with iterative structure refinement, *Nat. Struct. Biol. 6*, 458−463.
20. Murshudov, G. N., Vagin, A. A., Lebedev, A., Wilson, K. S., and Dodson, E. J. (1999) Efficient anisotropic refinement of macromolecular structures using FFT, *Acta Crystallogr. D55* (Part 1), 247−255.
21. (1994) The CCP4 suite: programs for protein crystallography, *Acta Crystallogr. D50*, 760−763.
22. McRee, D. E. (1999) XtalView/Xfit−A versatile program for manipulating atomic coordinates and electron density, *J. Struct. Biol. 125*, 156−165.
23. Vaguine, A. A., Richelle, J., and Wodak, S. J. (1999) SFCHECK: a unified set of procedures for evaluating the quality of macromolecular structure-factor data and their agreement with the atomic model, *Acta Crystallogr. D55* (Pt 1), 191−205.
24. Laskowski, R. A., MacArthur, M. W., Moss, D. S., and Thornton, J. M. (1993) PROCHECK: a program to check the stereochemical quality of protein structures, *J. Appl. Crystallogr. 26*, 283−291.
25. Delano, W. L. (2004) *The PyMOL molecular graphics system*, Delano Scientific, San Carlos, CA.
26. Qi, G., Lee, R., and Hayward, S. (2005) A comprehensive and non-redundant database of protein domain movements, *Bioinformatics 21*, 2832−2838.

27. Lee, R. A., Razaz, M., and Hayward, S. (2003) The DynDom database of protein domain motions, *Bioinformatics 19*, 1290−1291.
28. Hayward, S., and Berendsen, H. J. C. (1998) Systematic analysis of domain motions in proteins from conformational change; new results on citrate synthase and T4 lysozyme, *Proteins: Struct., Funct., Genet. 30*, 144−154.
29. Bellamacina, C. R. (1996) The nicotinamide dinucleotides binding motif: a comparison of nucleotide binding proteins, *FASEB J. 10*, 1257−1269.
30. Jang, M. S., Kang, N. Y., Kim, K. S., Kim, C. H., Lee, J. H., and Lee, Y. C. (2007) Mutational analysis of NADH-binding residues in triphenylmethane reductase from Citrobacter sp.strain KCTC 18061P, *FEMS Microbiol. Lett. 271*, 78−82.
31. Derman, A. I., Prinz, W. A., Belin, D., and Beckwith, J. (1993) Mutations that allow disulfide bond formation in the cytoplasm of *Escherichia coli*, *Science 262*, 1744−1747.

BI701428M